MULTI-LEVEL UNCERTAINTY QUANTIFICATION IN ADDITIVE MANUFACTURING

P. Nath, Z. Hu, and S. Mahadevan
Vanderbilt University, Nashville, TN 37235

Abstract

Quantifying the uncertainty in additive manufacturing (AM) process plays an important role in the quality control of additively manufactured products. This work presents an uncertainty quantification (UQ) framework to quantify the uncertainty of material microstructure due to multiple uncertainty (aleatory and epistemic) sources present in the AM simulation process. A multi-scale, multi-physics simulation model is first developed to simulate the melting and solidification processes. The melt pool profile obtained from macro-scale finite element analysis is coupled with a micro-scale cellular automata model to predict the microstructure evolution during solidification. Based on the simulation model, various sources of uncertainty are aggregated to quantify the uncertainty in the grain size distribution of the microstructure. The contributions of the various sources of uncertainty to the uncertainty of microstructure grain size distribution are analyzed using variance-based global sensitivity analysis. The results show that the proposed approach can effectively perform UQ of the AM process and the uncertainty in the grain size distribution is mainly affected by material properties and grain growth parameters.

1. Introduction

A major barrier to the widespread application of metal-based additive manufacturing (AM) techniques is the variability in the product quality. Variability is present at various stages of the manufacturing process. A good understanding of where the variability comes from and how to reduce the variability plays a critical role in guaranteeing the product quality of the AM process.

To improve the quality of products manufactured using the AM process, a trial and error approach for determining the optimal process parameters has often been adopted [1]. That is, the AM process is repeated numerous times to identify the relationship between process parameters and the product quality. Such a trial and error approach does not provide insights for generalization, and therefore has to be implemented every time a new design needs to be manufactured. This causes excessive energy and material wastage and significantly delays the product development process. Accurate modeling of the AM process can help optimize the process parameters without excessive energy and material wastage. However, the modeling process is affected by assumptions, approximations, and limited data. Therefore, the development of model-based quality control in AM also requires uncertainty quantification (UQ); as a result, UQ in AM has gained increasing attention in recent years [2, 3].

In recent decades, macro-scale finite element (FE) models as well as multi-scale multi-physics simulations have been studied to simulate the AM process [4-6]. These studies mainly concentrated on prediction and analysis of the melt pool geometry, and the influence of process parameters and materials on the melting process. In metal-based AM, the melt pool geometry affects the part microstructure that is the outcome of the melting-solidification process. The thermal history of the part and the microstructure evolution play a critical role in the macroscale properties of the manufactured part. Many multi-scale, multi-physics modeling studies have been

conducted on the evolution of the microstructure in the AM process. A finite element or finite difference macroscale model is generally used to capture the physics involved in the layer deposition system with a moving heat source leading to the estimation of the melt pool. Then the grain structure evolution during the solidification process is modeled using various approaches such as Monte Carlo sampling, phase field method, and cellular automata (CA) in the microscale [7]. The macro and the micro scale models are then coupled together to simulate the entire AM process [7, 8] and predict the microstructure of the manufactured part.

The above reviewed AM process modeling studies have mainly focused on deterministic process simulation. There are still many research issues that need to be solved before applying the simulation models to process optimization and thus achieve proactive quality control in AM. First, even though various multi-scale simulation models have been developed to study the material microstructure of components manufactured using AM, an overall framework that connects different types of simulations to the macroscale properties of the manufactured part and other quantities of interest (e.g. deformation, residual stress) is still missing. Second, different sources of uncertainty (physical variability, model approximations, and lack of knowledge about model parameters) are involved in different steps of the AM process. It is not clear how these uncertainty sources combine to affect the estimation of macroscale properties [9]. Third, with the multi-scale multi-physics simulation models getting more and more complicated, the computational effort required is also getting higher and higher. How to reduce the required computational effort in the AM process simulation and the associated UQ and process optimization analyses is thus an important research issue.

The focus of this paper is to develop an UQ framework for the AM process through multi-scale multi-physics simulation, connecting the simulated material microstructure with macroscale material properties, and considering various sources of uncertainty in each simulation model. The macroscale melt pool model is first coupled with the microscale solidification process model to simulate the material microstructure. The grain size distribution which is connected to the macroscale material property [10] is then analyzed. Based on the developed simulation model, various sources of uncertainties in the process such as variability of material properties of the powder, uncertainty regarding grain nucleation model parameters, and uncertainty regarding the grain growth model parameters are aggregated to quantify the uncertainty (i.e., variability plus lack of knowledge) regarding the final grain size distribution using a multi-level UQ method. A surrogate modeling method is employed to reduce the required computational effort in UQ and a variance-based global sensitivity analysis (GSA) method is used to identify the important process parameters that make significant contributions to the uncertainty of grain size distribution.

2. AM process simulation model

In this paper, the AM process is simulated using a coupled multi-scale multi-physics model, which includes two coupled models namely *melt pool simulation* and *microstructure simulation*. In this section we discuss each model and the coupling of the models in detail.

2.1. Melt pool simulation

In the melt pool simulation, the metal deposition process is modeled as a transient heat transfer problem. The governing equation for 3D transient heat transfer [11] is given by

$$\rho c\left[\frac{\partial T}{\partial t}+(-v)\frac{\partial T}{\partial t}\right]=K_c\left[\frac{\partial}{\partial x}\left(\frac{\partial T}{\partial x}\right)+\frac{\partial}{\partial y}\left(\frac{\partial T}{\partial y}\right)+\frac{\partial}{\partial z}\left(\frac{\partial T}{\partial z}\right)\right]+Q(x,y,z) \tag{1}$$

where Q is the volumetric heat source. K_c, c, ρ, v are respectively thermal conductivity, specific heat, density of the material, and the velocity of the heat source. The initial condition applied to the model is

$$T(x,y,z,0)=T_a \tag{2}$$

where T_a is the ambient temperature, and x, y, z are the spatial coordinates. Heat loss through convection is considered in the process.

The moving laser beam with power P is modeled as a Goldak heat source [8]. The heat is generated as a double ellipsoid which decays exponentially with distance from the center of the source as shown in Fig.1. This elliptical anisotropy is considered for more accurate description of melt pool [8].

$$Q(x,y,z)=\begin{Bmatrix}\dfrac{6\sqrt{3}f_fP}{abc_f\pi\sqrt{\pi}}\exp\left(\dfrac{-3x^2}{a^2}\right)\exp\left(\dfrac{-3y^2}{b^2}\right)\exp\left(\dfrac{-3z^2}{c_f{}^2}\right), z\geq 0\\ \dfrac{6\sqrt{3}f_rP}{abc_r\pi\sqrt{\pi}}\exp\left(\dfrac{-3x^2}{a^2}\right)\exp\left(\dfrac{-3y^2}{b^2}\right)\exp\left(\dfrac{-3z^2}{c_r{}^2}\right), z<0\end{Bmatrix} \tag{3}$$

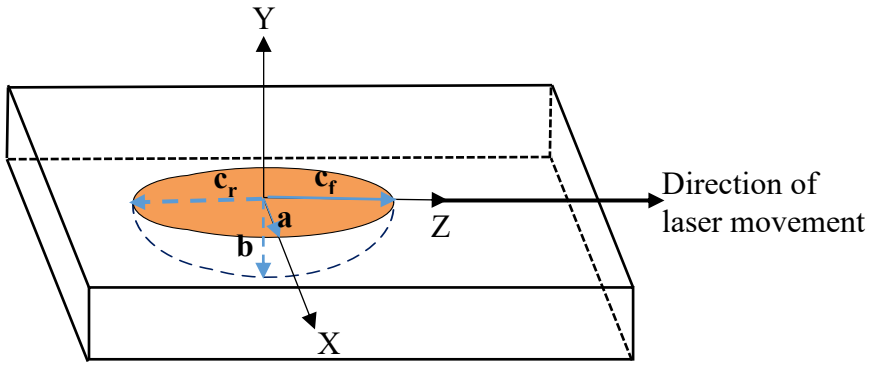

Figure 1. Schematic of heat source

Proportionality coefficients f_f and f_r representing fractions of the energy distributions in the front and rear parts of the ellipsoid are given as [8]

$$f_f=\frac{2}{1+\dfrac{c_r}{c_f}},\ f_r=\frac{2}{1+\dfrac{c_f}{c_r}} \tag{4}$$

The transient heat analysis is performed in the FE software Abaqus [12]. A user defined Fortran subroutine DFLUX is used to model the moving heat source. During the simulation process, the temperature field at the nodal locations for every time step is recorded. This temperature field is the input for CA model for solidification.

2.2. Cellular automata for microstructure

The modeling of microstructure evolution through the CA model consists of two main steps, namely *grain nucleation* and *grain growth*.

2.2.1 Grain nucleation

At characteristic undercooling, heterogeneous nucleation occurs. The nucleation sites are at the mold wall and the bulk of the melt. Nucleation density depends on the degree of undercooling. The nucleation grain density $n(\Delta T)$ in the melt pool is represented by a Gaussian function [13].

$$\begin{aligned} n(\Delta T) &= \int_0^{\Delta T} \frac{dn}{d(\Delta T)} d(\Delta T) \\ &= \frac{n_{\max}}{\Delta T_\sigma \sqrt{2\pi}} \int_0^{\Delta T} \exp\left[-\frac{(\Delta T - \Delta T_N)^2}{2(\Delta T_\sigma)^2} \right] d(\Delta T) \end{aligned} \tag{5}$$

where ΔT_N and ΔT_σ mean undercooling and standard deviation respectively of the grain density distribution, $n_{\max}$ is the maximum nucleation density. These parameters are generally obtained from experiments and grain size measurements. In the present work, these values are assumed for demonstration purposes.

At each time step, the undercooling at the nodes is obtained from the macroscale model. The nucleation density is calculated using Eq. (5). If the nucleation probability (p) given by Eq. (6) is greater than or equal to a random number $r(0 \le r \le 1)$, then cell is considered to be nucleated.

$$p = \delta n V_{CA} \tag{6}$$

where δn is the grain density increase between two subsequent time steps, and V_{CA} is the volume of one CA cell [13].

2.2.2 Grain growth

The dendritic growth depends on the undercooling. The total undercooling (ΔT) is the sum of solutal undercooling (ΔT_C), thermal undercooling (ΔT_T), kinetic undercooling (ΔT_K), and curvature undercooling (ΔT_R) [13].

$$\Delta T = \Delta T_C + \Delta T_T + \Delta T_K + \Delta T_R \tag{7}$$

Only thermal undercooling is undercooling considered in the present work. Based on this assumption, the dendritic growth velocity equation [14] is assumed as a power function of thermal undercooling.

Cellular automaton [15] is used to simulate grain growth. In this work, regular square lattice and Moore third order neighborhood (see Fig. 2(b)) are considered. Each cell can be in one of the three states: liquid, mushy, or solid, with a state index of 0, 1, and 2 respectively. A mushy cell is partially liquid and partially solid. The CA model enables simulating complex grain morphology in a simple and efficient manner by approximating the dendrite morphology by a dendrite envelop represented as a square [13]. The half diagonals of the square correspond to the crystallographic grain directions <10>. The grains grow along these directions as shown in Fig. 2(a). When a cell is nucleated, it is assigned a crystallographic orientation angle θ between the CA axis and preferred grain growth direction. Using the CA grain growth algorithm [16], the grain growth is simulated in the 2D domain space. The envelope grows and captures neighboring cells. The captured cell is assigned the same θ as the growing grain. A grain stops growing when all the cells in its neighborhood are captured. At each time step, new cells are nucleated and captured. The process is repeated till the microstructure fills the computational domain. Thus the evolution of microstructure is simulated.

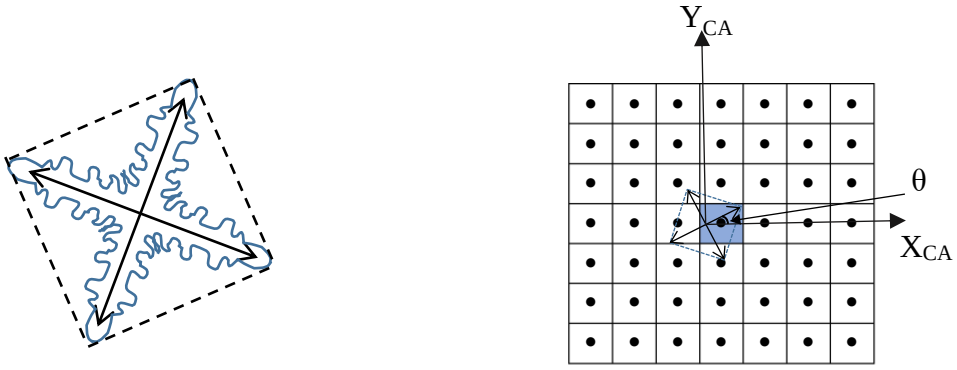

(a) Schematics of grain morphology (b) Third order Moore neighborhood

Figure 2. Components of CA model

2.3 Coupling of macroscopic and microscopic models

There are two coupling modes between macroscopic FE model and the microscopic CA model: weak coupling mode and full coupling mode [17]. Weak coupling involves interpolation of temperature. The temperature field obtained from the coarse meshed FE model for macro time steps is linearly interpolated in both space and time dimensions to get temperature field inputs that fulfill CA growth criterion. Full coupling is more accurate than weak coupling. It involves recalculation of temperature and solid fraction of the macroscale nodes after each micro time step using micro enthalpy scheme. More details on the coupling modes can be found in Ref. [17]. The main advantage of weak coupling calculation mode is that the CA calculations can be done after the completion of the FE calculation.

2.4 Summary of the simulation process

The simulation process described above is summarized in the form of a flowchart in Fig. 3. From the simulated microstructure, grain size distribution is obtained and the standard deviation of the grain size distribution is considered as the macroscale quantity of interest.

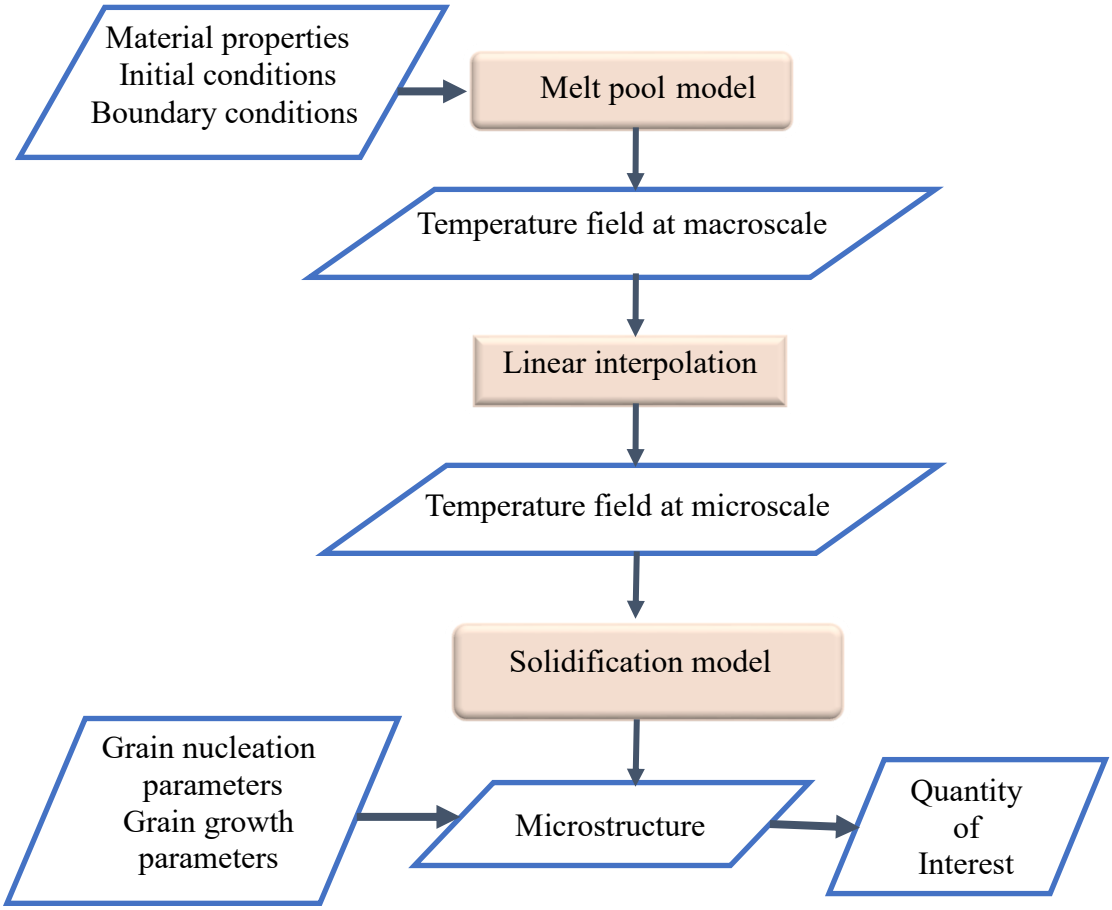

Figure 3. Flowchart of the simulation

3.Uncertainty quantification of the material properties in AM

The additive manufacturing process discussed in Section 2 has various sources of uncertainties at each level of the simulation shown in Fig. 3. In this section, we first analyze the uncertainty sources in the simulation models and then discuss the methodology for the aggregation and propagation of the uncertainty sources.

3.1. Uncertainty sources analysis

The sources of uncertainty in the simulation model can be grouped under (a) uncertainties in the macroscale melt pool model, and (b) uncertainties in the microscale solidification model.

The melt pool geometry and the corresponding temperature field, which is the output of the macroscale model, are dependent upon the input parameters of the model. The material properties of the powder such as density, conductivity, specific heat, Young's modulus etc., are temperature-dependent. Variability of these material properties causes variability of the temperature field.

At the microscale model level, there are uncertainties regarding the grain nucleation parameters such as mean and standard deviation of the grain density distribution, and maximum grain density. There are also uncertainties regarding grain growth parameters such as the coefficients of the power law considered for grain velocity. These different sources of uncertainties aggregate and propagate to bring about uncertainty regarding the microstructure.

3.2 Surrogate Model

As discussed previously, the grain microstructure is dependent on various uncertain parameters. To understand the effect of these, we need to run the simulation model repeatedly by varying the model parameters. However, these computational models are expensive. Thus surrogate models, which are cheap approximate models of the original model, need to be built to replace the computationally expensive physics-based simulation models. There are different kinds of surrogates available for the purpose, such as polynomial chaos expansion, Gaussian process, radial basis functions, etc. In this paper, a Kriging surrogate model (i.e., Gaussian process model) is created for the FE melt pool model. As the CA solidification model is not very expensive, the original simulation model is used for solidification.

3.2.1 Kriging surrogate model

A Kriging model approximates a response function $G(\mathbf{d})$ as [18, 19]

$$\hat{G}(\mathbf{d}) = \mathbf{h}(\mathbf{d})^T \boldsymbol{\alpha} + Z(\mathbf{d}) \tag{8}$$

where $\mathbf{h}(\mathbf{d})$ are the trend functions, $\boldsymbol{\alpha}$ are the trend coefficients, and $Z(\mathbf{d})$ is a zero mean Gaussian process and covariance $Cov[z(\mathbf{d}_i), z(\mathbf{d}_j)] = \sigma_z^2 K(\mathbf{d}_i, \mathbf{d}_j)$, where σ_z^2 is the process variance and $K(\cdot,\cdot)$ is the correlation function.

For an untrained point $\mathbf{d}_*$, the mean value of the prediction is given by [18, 19]

$$\mu(\mathbf{d}_*) = \mathbf{h}^T(\mathbf{d}_*)\boldsymbol{\alpha} + \mathbf{K}_*\mathbf{K}^{-1}(\mathbf{y}_t - \mathbf{H}\boldsymbol{\alpha}) \tag{9}$$

where $\mathbf{K}$ is the correlation matrix with elements $K(\mathbf{d}_i, \mathbf{d}_j)$, $i, j = 1, 2, ..., n$, $\mathbf{H} = [\mathbf{h}(\mathbf{d_1})^T, \mathbf{h}(\mathbf{d}_2)^T, \cdots, \mathbf{h}(\mathbf{d}_n)^T]^T$, $\boldsymbol{\alpha} = (\mathbf{H^T K^{-1} H})^{-1}\mathbf{H^T K^{-1} g}$ with $\mathbf{g} = [g(\mathbf{d}_1), g(\mathbf{d}_2), \cdots, g(\mathbf{d}_n)]^T$, $\mathbf{K}_* = \begin{bmatrix} R(\mathbf{d}_*, \mathbf{d}_1) & R(\mathbf{d}_*, \mathbf{d}_2) & \cdots & R(\mathbf{d}_*, \mathbf{d}_n) \end{bmatrix}$ in which $\mathbf{d}_1, \cdots, \mathbf{d}_n$ are the training points, and n is the number of training points.

The mean square error (MSE) of the prediction is given by [18, 19]

$$\text{MSE}(\mathbf{d}_*) = \sigma_z^2\{1 - \mathbf{K}_*{}^T\mathbf{R}^{-1}\mathbf{K}_* + [\mathbf{H}^T\mathbf{R}^{-1}\mathbf{K}_* - \mathbf{h}(\mathbf{d}_*)]^T(\mathbf{H}^T\mathbf{R}^{-1}\mathbf{H})^{-1}[\mathbf{H}^T\mathbf{R}^{-1}\mathbf{K}_* - \mathbf{h}(\mathbf{d}_*)]\} \tag{10}$$

$$\sigma_z^2 = \frac{(\mathbf{g} - \mathbf{H}\boldsymbol{\alpha})^T\mathbf{R}^{-1}(\mathbf{g} - \mathbf{H}\boldsymbol{\alpha})}{n} \tag{11}$$

In this paper, we build a surrogate for the macroscale melt pool model to estimate the temperature field of the melt pool given the uncertainty in the material properties. As the

temperature field is a high-dimensional response, singular value decomposition (SVD) [20] is employed to map the high-dimensional response to a low-dimensional latent space, and the surrogate model is constructed in the low-dimensional space.

3.2.2 Singular value decomposition (SVD)

The temperature field data is denoted as $w(\mathbf{p},\boldsymbol{\xi}):\Omega\times\Psi\rightarrow R$ over a q-dimensional spatial domain Ω of $\mathbf{p}=[p_1, p_2, \cdots, p_q]$, where $\boldsymbol{\xi}$ indicates different realizations over the spatial domain. Given m data points over the spatial domain Ω for n_t realizations, we have the temperature field data matrix as

$$\begin{aligned}\mathbf{w} &= [w(\xi_1), w(\xi_2), \ldots, w(\xi_{n_t})] \in R^{m\times n_t},\\ &= \{[w(\mathbf{p}^{(i)},\boldsymbol{\xi}_j)]\}, \forall i=1,2,...,m;\ j=1,2,...,n_t,\end{aligned} \tag{12}$$

where $\mathbf{w}(\boldsymbol{\xi}_j)=[w(\mathbf{p}^{(1)},\boldsymbol{\xi}_j), w(\mathbf{p}^{(2)},\boldsymbol{\xi}_j),..., w(\mathbf{p}^{(m)},\boldsymbol{\xi}_j)]^T$ and $\mathbf{d}_i, i=1,2,...,m$ is the i^{th} observation location.

The data matrix $\mathbf{w}$ is decomposed by SVD as $\mathbf{w}=\mathbf{VMU}^T$, where $\mathbf{V}$ is a $n_t\times n_t$ orthogonal matrix, $\mathbf{U}$ is a $m\times m$ orthogonal matrix and $\mathbf{M}$ is a $n_t\times m$ rectangular diagonal matrix with non-negative real numbers $\boldsymbol{\lambda}=[\lambda_1,\lambda_2,\ldots,\lambda_k]$ (called singular values) along the diagonal arranged in descending order, in which $k=\min(m,n_t)$. Defining another matrix as $\boldsymbol{\gamma}=\mathbf{VM}$, the original temperature field data matrix can be represented as $\mathbf{w}(\xi_i)^T=\boldsymbol{\gamma}_{i:}\mathbf{U}^T=\sum_{j=1}^{r}\gamma_{ij}\boldsymbol{\varphi}_j$, where $\boldsymbol{\gamma}_{i:}$ stands for the *i*-th row of $\boldsymbol{\gamma}$, $\mathbf{w}(\xi_i)^T$ is the *i*-th row of $\mathbf{w}$, γ_{ij} is the element of $\boldsymbol{\gamma}$ at *i*-th row and *j*-th column, $\boldsymbol{\varphi}_j$ (*j*-th row of $\mathbf{U}^T$) is the *j*-th important feature vector used to approximate $\mathbf{w}$, and *r* is the number of important features used. The number of important features *r* is determined based on the magnitudes of the singular values λ [21].

3.2.3 Surrogate modeling of the temperature field using Kriging and SVD

A Kriging surrogate model is built for the low-dimensional latent response obtained from SVD and used for the prediction of the original high-dimensional temperature field response. For the uncertain parameters $\boldsymbol{\theta}$, n_s training points are generated. The response $\mathbf{y}$ is obtained for each training point from the original melt pool simulation model. SVD is performed on the reshaped temperature field data matrix given by

$$\mathbf{y}_{total}=\begin{bmatrix} y(\mathbf{p}^{(1)},\boldsymbol{\theta}^{(1)}) & y(\mathbf{p}^{(1)},\boldsymbol{\theta}^{(2)}) & \cdots & y(\mathbf{p}^{(1)},\boldsymbol{\theta}^{(n_s)}) \\ y(\mathbf{p}^{(2)},\boldsymbol{\theta}^{(1)}) & y(\mathbf{p}^{(2)},\boldsymbol{\theta}^{(2)}) & \cdots & y(\mathbf{p}^{(2)},\boldsymbol{\theta}^{(n_s)}) \\ \vdots & \vdots & \ddots & \vdots \\ y(\mathbf{p}^{(m)},\boldsymbol{\theta}^{(1)}) & y(\mathbf{p}^{(m)},\boldsymbol{\theta}^{(2)}) & \cdots & y(\mathbf{p}^{(m)},\boldsymbol{\theta}^{(n_s)}) \end{bmatrix}^T \tag{13}$$

Based on SVD, the temperature field response given in Eq.(13) is reconstructed as

$$y_{total}(\mathbf{p}^{(k)}, \boldsymbol{\theta}^{(i)}) \approx \mu(\mathbf{p}^{(k)}) + \sum_{j=1}^{r} \gamma_j(\boldsymbol{\theta}^{(i)}) U_j(\mathbf{p}^{(k)}), \forall i = 1, 2, \cdots, n_s; k = 1, 2, \cdots, n_p; \quad (14)$$

where $\mu(\mathbf{p}^{(k)})$ is the mean value at location $\mathbf{p}^{(k)}$ and $U_j(\mathbf{p}^{(k)})$ is the value of $\mathbf{U}_j$ at spatial location $\mathbf{p}^{(k)}$. Surrogate models are constructed for $\gamma_1, \gamma_2, \cdots, \gamma_r$ using Kriging. Replacing γ_j by $\hat{\gamma}_j$ in Eq. (14), we have

$$y_{total}(\mathbf{p}^{(k)}, \boldsymbol{\theta}^{(i)}) \approx \mu(\mathbf{p}^{(k)}) + \sum_{j=1}^{r} \hat{\gamma}_j(\boldsymbol{\theta}^{(i)}) U_j(\mathbf{p}^{(k)}), \forall k = 1, 2, \cdots, n_p; \quad (15)$$

in which $\hat{\gamma}_j(\boldsymbol{\theta}^{(i)})$ stands for the surrogate model of γ_j.

The obtained surrogate model is used to predict the temperature field response which is an input to the solidification model.

3.3. Multilevel Uncertainty Propagation

The uncertainty propagation throughout the process is represented in Fig.4.

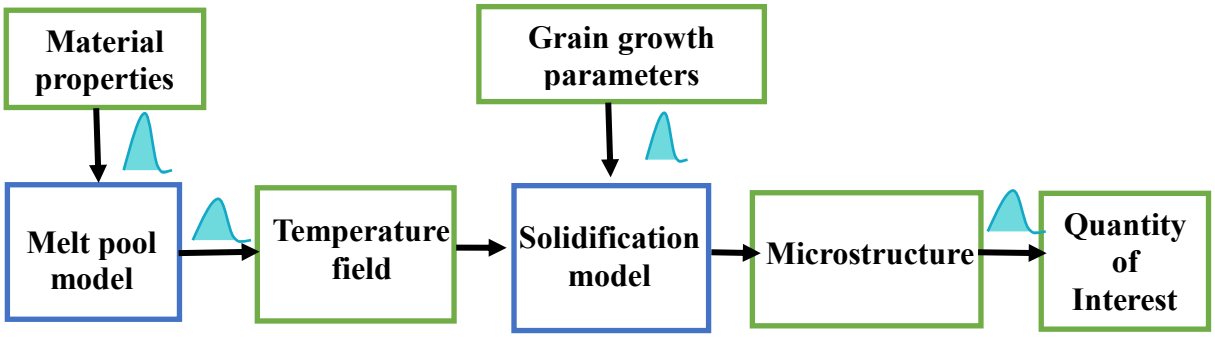

Figure 4. Multi-Level Uncertainty propagation

3.4. Global Sensitivity Analysis

As discussed earlier, uncertainty in the macro-level quantity of interest comes from different sources. To manage and reduce the uncertainty, it is important to ascertain the contribution from each source. Global sensitivity analysis is a valuable tool for this purpose. The contribution of input θ to the variance of output Q is quantified using Sobol' indices. The first order index S_I measures the individual contribution of the input variable θ^i, and the total effects index S_T measures the contribution of an input variable in combination with other variables.

$$S_I = \frac{V_{\theta_i}(E_{\theta_{\sim i}}(Q \mid \theta_i))}{V(Q)} \quad (16)$$

$$S_T = \frac{E_{\theta_{\sim i}}(V_{X_i}(Q \mid \theta_{\sim i}))}{V(Q)} \quad (17)$$

where $E[\bullet]$ and $V[\bullet]$ represent expectation and variance operators respectively. Using the above equations, the relative contributions of different sources of uncertainty on the uncertainty in the macro-level QoI are determined.

In summary, the proposed multi-level UQ framework for the AM process consists of the following steps:

- Development of the deterministic AM simulation model;
- Uncertainty sources analysis;
- Surrogate modeling of the melt pool model;
- Uncertainty propagation analysis through the AM simulation model; and
- Global sensitivity analysis of the output QOI (grain size distribution in this study).

Next, an illustrative example is used to demonstrate the above proposed UQ framework.

4. Illustrative example

Consider a substrate of size 2000μm×2000μm×100μm. We want to deposit a layer of 500μm×1000μm×50μm on the substrate and examine the microstructure. The description of the models is given below.

4.1. Melt pool simulation

A finite element model of the part is created in the commercial software Abaqus [12] as shown in Fig. 5(a). The substrate is assumed to be fixed at the bottom and the ambient temperature is set to the room temperature of 298 K. Heat loss due to convection is considered during the process. A moving Goldak heat source is defined using DFLUX subroutine to simulate the melting of powder by the laser [8] as shown in Fig. 5(b). A finer mesh increases the computation time substantially. Therefore the part was finely meshed only at the areas of interest, i.e., the powder layer and the portion of the substrate adjacent to the powder layer. Figure 5(c) shows the mesh comprising of 8-noded linear heat transfer brick element. Figure 6 shows the contour of the melt pool.

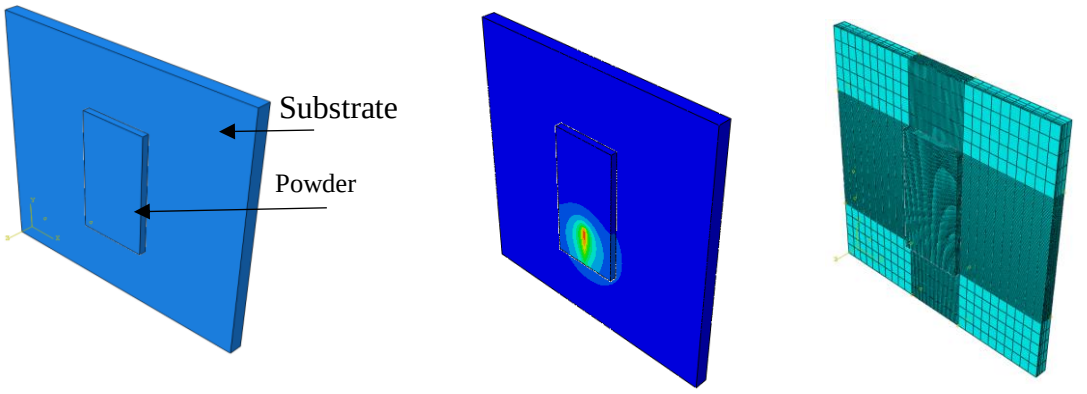

(a) Geometry of the model (b) Laser heat source (c) Meshed model

Figure 5. Finite element simulation

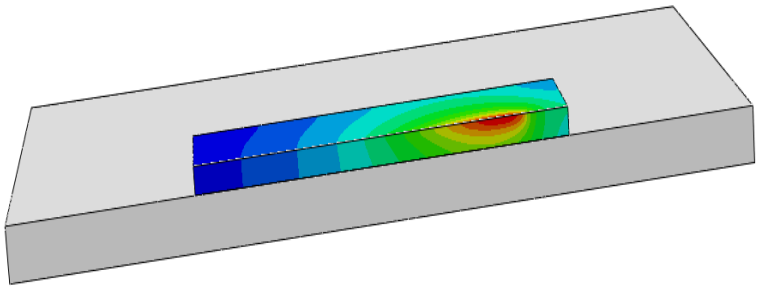

Figure 6. Simulated melt pool

4.2 Surrogate modeling of melt pool

Following the procedure described in Sec. 3.2., the Kriging surrogate model is constructed to replace the FEA model for the temperature field, using 50 training points generated by Latin hypercube sampling. The temperature response is reconstructed using the first 10 important features. The reconstructed response has less than 1% difference when compared to the original simulation as shown in Fig. 7.

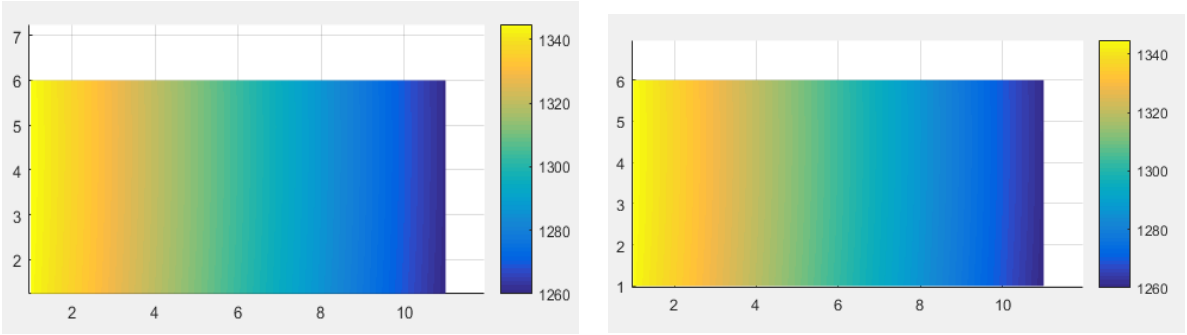

(a) Reconstructed response (b) Original response

Figure 7. Comparison of original and reconstructed temperature response

4.3 Microstructure simulation

The CA algorithm discussed in Sec 2.2 is implemented for this example. The computational domain considered from FEA model is further subdivided to suit the requirements of the CA algorithm. The temperature field obtained using the surrogate model at the nodes of the macroscopic model is linearly interpolated in both space and time dimensions to serve as input for the CA model. The microstructure for the entire computational domain is simulated as shown in Fig. 8.

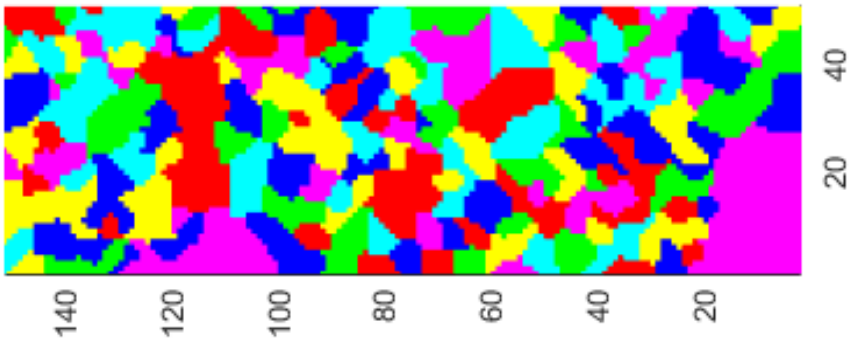

Figure 8. Simulated microstructure by CA algorithm

4.4.1 Modeling of uncertainty sources

For the melt pool model, we consider the material properties, namely, density (ρ), conductivity (K_c), and specific heat (c), as the uncertain model parameters. As these parameters are temperature dependent [7], a second degree polynomial of the form $m_1T^2 + m_2T + m_3$ is fitted though the available experimental data points. Thus, there are a total of 9 uncertain parameters in the macroscale FEA model, i.e., $\theta^m = [\mathbf{m_1}, \mathbf{m_2}, \mathbf{m_3}]$.

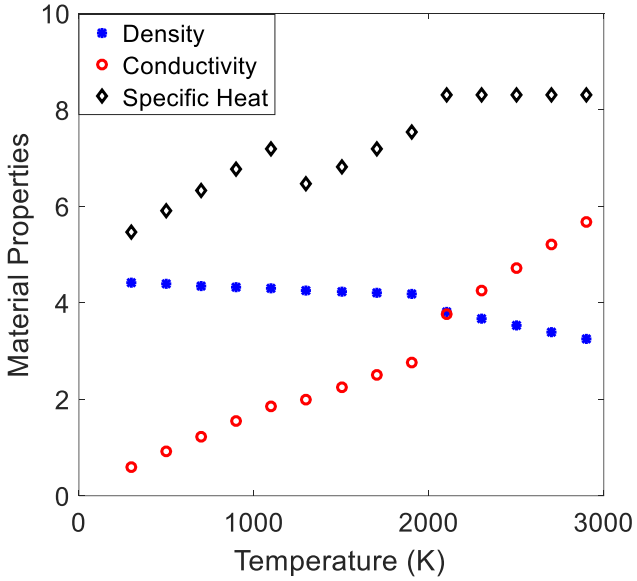

Figure 9. Temperature dependent material properties

In the solidification model, the grain growth velocity is assumed to be a power law of the form $V_g = A_g \times (\Delta T)^{b_g}$. The parameters A_g and b_g are considered uncertain along with the solidus and liquidus temperatures T_s and T_L. Thus the uncertain parameters are $\theta^s = [T_L, T_S, A_g, b_g]$. The probability distributions and statistics considered for the uncertain variables are shown in Tables 1 and 2.

Table 1. Random variables of melt pool model

Variable	m_1^{ρ} $\times 10^{-16}$	m_2^{ρ} $\times 10^{-13}$	m_3^{ρ} $\times 10^{-9}$	$m_1^{K_c}$ $\times 10^{-6}$	$m_2^{K_c}$ $\times 10^{-3}$	$m_3^{K_c}$	m_1^{c}	m_2^{c} $\times 10^{5}$	m_3^{c} $\times 10^{8}$
Distribution	Gaussian								
Mean	-2.2	2.6	4.3	4.3	5.5	5.39	-17	1.65	5.13
Standard deviation	0.11	0.26	0.02	0.35	0.55	0.53	1.7	0.08	0.05

Table 2. Random variables of solidification model

Variable	T_L	T_S	A_g	b_g
Distribution	Uniform			
Minimum	1910	990	7.5	1.42
Maximum	1930	1010	7.6	1.44

Of the above uncertain parameters, T_L and T_S are considered epistemic, i.e., they have fixed values which are unknown; this uncertainty is lack of knowledge and is reducible when more information is available. Following a Bayesian perspective, such epistemic uncertainty is represented by a prior probability distribution, and is updated to a posterior distribution with new data. The other uncertain parameters are assumed to vary across multiple manufactured parts and are considered to be aleatory. Uncertainty in the grain nucleation parameters is not considered in this example. Also, we have not considered any model errors. Including model uncertainty in the analysis is one of our future work.

4.4.2 Uncertainty propagation

The uncertainty in the model parameters leads to uncertainty in the microstructure which in turn causes uncertainty in the macroscale QoI. For this work, we consider the grain size distribution to be the QoI. Figure 10 illustrates the propagation of uncertainty at multiple levels of the simulation model.

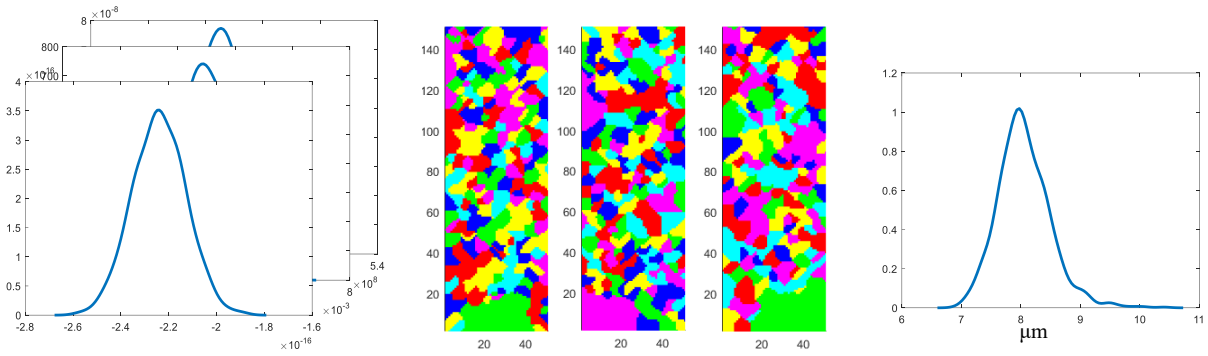

(a) Model parameter uncertainty

(b) Uncertainty in the microstructure

(c) Uncertainty in QoI (Std. Dev. of Grain size)

Figure 10. Uncertainty propagation from model parameters to QoI

4.5 Global sensitivity analysis results

The contributions of various sources of uncertainty to the standard deviation of the grain size distribution is analyzed using GSA. The first order Sobol' indices from the sensitivity analysis are presented in Fig. 11. It is observed that the material parameters of the melt pool model and the grain growth parameters of the solidification model make significant contribution to uncertainty in the standard deviation of grain size distribution. The epistemic uncertainties (T_L and T_S) are less influential, and can be reduced by collecting more data from experiments.

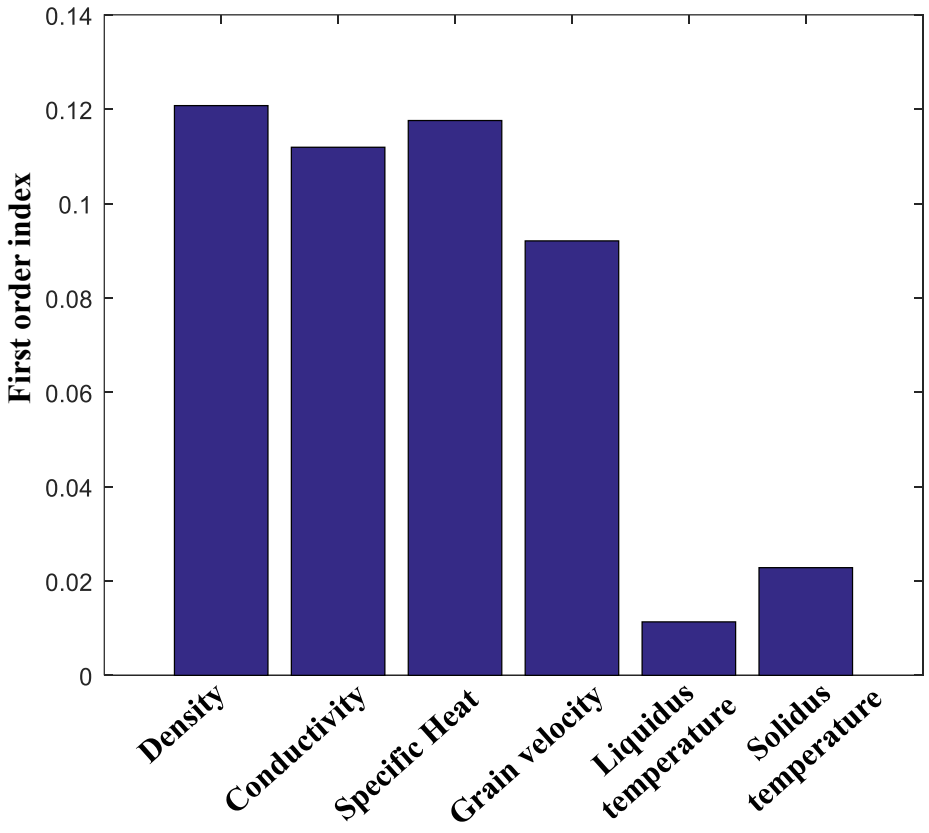

Figure 11. First order indices from GSA

5. Conclusion

Quality control in additive manufacturing can be achieved by process optimization for variation control. A trial and error approach to process parameter optimization is expensive and not generalizable, therefore computational models are used. However, such model-based quality control requires quantification of uncertainty, arising from multiple modeling and data sources and natural variability. In this paper, forward propagation of uncertainty through the models at multiple levels has been studied. It is followed by GSA to analyze the contribution of various sources of uncertainty.

Future work can extend the proposed approach to two types of inverse problems. The first inverse problem is to reduce the uncertainty by updating the model parameters using experimental data; an associated additional problem is to design the experiments such that the information gain is maximized. The second inverse problem is to pursue optimization under uncertainty of the manufacturing process parameters such as laser power, laser velocity, layer thickness etc., in order to reduce the product variability in terms of geometry, material properties and other performance and quality measures.

Acknowledgement

This study was supported by funds from the National Science Foundation (Grant No.1404823, CDSE Program). The support is gratefully acknowledged.

References

[1] Kobryn, P., and Semiatin, S., 2001, "The laser additive manufacture of Ti-6Al-4V," JOM Journal of the Minerals, Metals and Materials Society, 53(9), pp. 40-42.
[2] Hu, Z., and Mahadevan, S., 2017, "Uncertainty quantification in prediction of material properties during additive manufacturing," Scripta Materialia, 135, pp. 135-140.
[3] Hu, Z., and Mahadevan, S., 2017, "Uncertainty quantification and management in additive manufacturing: current status, needs, and opportunities," The International Journal of Advanced Manufacturing Technology, pp. 1-20.
[4] Shen, N., and Chou, K., "Thermal modeling of electron beam additive manufacturing process: Powder sintering effects," Proc. ASME 2012 International Manufacturing Science and Engineering Conference collocated with the 40th North American Manufacturing Research Conference and in participation with the International Conference on Tribology Materials and Processing, American Society of Mechanical Engineers, pp. 287-295.
[5] Fu, C., and Guo, Y., "3-Dimensional Finite Element Modeling of Selective Laser Melting Ti-6Al-4V Alloy," Proc. Solid Freeform Fabrication Symposium 2014 Proceedings.
[6] Cheng, B., and Chou, K., "Melt pool geometry simulations for powder-based electron beam additive manufacturing," Proc. 24th Annual International Solid Freeform Fabrication Symposium-An Additive Manufacturing Conference, Austin, TX, USA.
[7] Zhang, J., Liou, F., Seufzer, W., and Taminger, K., 2016, "A coupled finite element cellular automaton model to predict thermal history and grain morphology of Ti-6Al-4V during direct metal deposition (DMD)," Additive Manufacturing, 11, pp. 32-39.
[8] Zinoviev, A., Zinovieva, O., Ploshikhin, V., Romanova, V., and Balokhonov, R., 2016, "Evolution of grain structure during laser additive manufacturing. Simulation by a cellular automata method," Materials & Design, 106, pp. 321-329.
[9] Cai, G., and Mahadevan, S., 2016, "Uncertainty quantification of manufacturing process effects on macroscale material properties," International Journal for Multiscale Computational Engineering, 14(3).
[10] Lehto, P., Remes, H., Saukkonen, T., Hänninen, H., and Romanoff, J., 2014, "Influence of grain size distribution on the Hall–Petch relationship of welded structural steel," Materials Science and Engineering: A, 592, pp. 28-39.
[11] Reddy, J. N., and Gartling, D. K., 2010, The finite element method in heat transfer and fluid dynamics, CRC press.
[12] Hibbitt, Karlsson, and Sorensen, 2001, ABAQUS/standard user's Manual, Hibbitt, Karlsson & Sorensen.
[13] Rappaz, M., and Gandin, C.-A., 1993, "Probabilistic modelling of microstructure formation in solidification processes," Acta metallurgica et materialia, 41(2), pp. 345-360.
[14] Zhou, K., and Wei, B., 2016, "Determination of the thermophysical properties of liquid and solid Ti–6Al–4V alloy," Applied Physics A, 122(3), pp. 1-5.
[15] Cochinos, R., 2000, "Introduction to the theory of cellular automata and one-dimensional traffic simulation," Página web http://www. theory. org/complexity/traffic/[Consulta em Outubro de 2005].
[16] Zinovieva, O., Zinoviev, A., Ploshikhin, V., Romanova, V., and Balokhonov, R., 2015, "A solution to the problem of the mesh anisotropy in cellular automata simulations of grain growth," Computational Materials Science, 108, pp. 168-176.
[17] Gandin, C.-A., Desbiolles, J.-L., Rappaz, M., and Thevoz, P., 1999, "A three-dimensional cellular automation-finite element model for the prediction of solidification grain structures," Metallurgical and Materials Transactions A, 30(12), pp. 3153-3165.
[18] Rasmussen, C., and Williams, C., 2006, "Gaussian Processes for Machine Learning," Gaussian Processes for Machine Learning.
[19] Lophaven, S. N., Nielsen, H. B., and Søndergaard, J., 2002, "DACE-A Matlab Kriging toolbox, version 2.0."
[20] Chatterjee, A., 2000, "An introduction to the proper orthogonal decomposition," Current science, 78(7), pp. 808-817.
[21] Xu, P., 1998, "Truncated SVD methods for discrete linear ill-posed problems," Geophysical Journal International, 135(2), pp. 505-514.